

Processing of Continuous Non-Crosslinked Collagen Fibers for Microtissue Formation at the Muscle-Tendon Interface

Kim Sarah Koeck, Sahar Salehi, Martin Humenik, and Thomas Scheibel*

One of the main components of the extracellular matrix (ECM) in natural tissues is collagen. Therefore, there has been a strong focus on processing of collagen for biomaterials application in tissue engineering such as in anisotropic tissues like muscles and tendons. To achieve native-like mechanical properties of the *in vitro* processed collagen, various crosslinking methods have been tested, but the used crosslinkers often do not yield sufficient mechanical properties or induce considerable inflammatory reactions. Here, good mechanical stability of collagen fibers is achieved by self-assembly during wet-spinning without the need of additional crosslinkers. The produced endless collagen fibers show fibril alignment within the fiber with a typical D-band pattern and a periodicity of approximately 67 nm, which is unique for fibril-forming collagens. Furthermore, the collagen fibers are processed into hierarchical assemblies using textile-engineering techniques. The woven assemblies are shown to be excellent substrates for the formation of muscle microtissue with long, aligned, and contractile myofibers. Such constructs are highly important at the muscle-tendon-junction (MTJ) and therefore myoblasts and fibroblasts are co-cultured to develop an MTJ-model.

1. Introduction

A close look at the architecture of muscle and tendon indicates the importance of fibrillar, hierarchical structures and their role in generating proper physical and mechanical properties. Therein, as many other tissues, collagen type I fibers are responsible for providing the physiological and mechanoactive environment to coordinate cellular activity.^[1–3] There are at least 28 different collagen types in vertebrates, of which most self-assemble into fibrils by an entropy-driven process caused by the loss of solvent molecules from the surface leading to an energetically minimized area/volume ratio.^[2,4] In tissue engineering, often collagen type I-based biomaterials and fiber processing techniques are used to mimic the natural micro-/nanostructure of different tissues.^[2,5,6] As collagen is biocompatible, biodegradable, and shows low immuno-

genicity,^[3,7] techniques such as electrospinning, self-assembly, and wet spinning have been used to process collagen into fiber morphologies.^[8–10,5,11] In wet spinning approaches collagen is first dissolved in a suitable solvent, and fiber formation occurs as soon as the solution is extruded into a coagulation bath,^[12–14] consisting of a poor-solvent (non-solvent) or a non-solvent/solvent mixture. Coagulation occurs due to neutralization, dehydration, and/ or ion exchange.^[15] However, the wet-spinning of collagen fibers, as of yet, has failed to yield nature-like structures, bioactivities, or mechanical strength.^[16] Previous studies on the production of collagen fibers out of diluted acids^[12,13,17–21] upon coagulation in pure ethanol,^[12] phosphate buffered saline (PBS) buffers,^[22] or polyethylene glycol (PEG)-containing buffers,^[11,17,19,21,23] required additional chemical crosslinking using genipin,^[13] glutaraldehyde,^[13] 1-ethyl-3-(3-dimethylaminopropyl) carbodiimide/*N*-hydroxysuccinimide (EDC/NHS),^[12,24] glyoxal,^[23] or formaldehyde^[20] to ensure acceptable mechanical properties. While previous studies focused on crosslinking strategies to enhance the mechanical properties of spun fibers, emphasis on determining the effect of these crosslinking processes on host tissue responses was neglected. Such crosslinking agents are mostly cytotoxic and have to be thoroughly removed before collagen fibers can be used in context with living cells.^[25] Furthermore, insufficient crosslinking can result in lower tensile strength.^[23] Delgado et al. discussed the response of host tissue and macrophages to different crosslinking methods and densities for stabilizing collagen-based scaffolds. *In vitro* and *in vivo* data showed that such

K. S. Koeck, S. Salehi, M. Humenik, T. Scheibel

Department of Biomaterials

University of Bayreuth

Prof.-Rüdiger-Bormann Str. 1, 95447 Bayreuth, Germany

E-mail: thomas.scheibel@bm.uni-bayreuth.de

T. Scheibel

Bayreuther Zentrum für Kolloide und Grenzflächen (BZKG)

University of Bayreuth

Universitätsstraße 30, 95447 Bayreuth, Germany

T. Scheibel

Bayreuther Zentrum für Molekulare Biowissenschaften (BZMB)

University of Bayreuth

Universitätsstraße 30, 95447 Bayreuth, Germany

T. Scheibel

Bayreuther Materialzentrum (BayMAT)

University of Bayreuth

Universitätsstraße 30, 95447 Bayreuth, Germany

T. Scheibel

Bayerisches Polymerinstitut (BPI)

University of Bayreuth

Universitätsstraße 30, 95447 Bayreuth, Germany

 The ORCID identification number(s) for the author(s) of this article can be found under <https://doi.org/10.1002/adfm.202112238>.

© 2021 The Authors. Advanced Functional Materials published by Wiley-VCH GmbH. This is an open access article under the terms of the Creative Commons Attribution-NonCommercial License, which permits use, distribution and reproduction in any medium, provided the original work is properly cited and is not used for commercial purposes.

DOI: 10.1002/adfm.202112238

chemical crosslinking methods alter the normal wound healing process, even at low concentrations. Using higher concentrations resulted in M1 macrophage response and inhibition of M2 macrophage polarization, reduced cell infiltration, increased proinflammatory cytokine expression, chronic wounds, peri-implantation fibrosis, and delayed wound healing.^[26]

We previously showed the production of collagen microfibers with good mechanical properties without using crosslinking agents. However, the mechanical properties were measured only in dry state and not in a hydrated one.^[17] Non-crosslinked collagen fibers in a hydrated state are known to be less mechanically stable.^[13,23] Further, in most tissue engineering applications such as large-scale musculoskeletal tissue regeneration, collagen-based scaffolds are more common than single fibers. Textile techniques (e.g., weaving and braiding) allow to produce fine-tuned tissue-like constructs mimicking the microarchitecture of the native tissues as well as enhancing the stability of the collagen fibers in wet state.^[27] Such techniques offer control of the fabricated constructs' size, shape, porosity, and of mechanical properties of the fabricated constructs to mimic that of muscles, tendons, or their interface.^[11,28] Therefore, we here extended our processing set-up to yield hierarchically structured collagen constructs.

Musculoskeletal tissues (muscle, muscle–tendon junction (MTJ), tendon, etc.) are anisotropic tissues with specific collagen fiber orientations, which provide stability, integrity, and mobility to the body.^[5] The native MTJ comprises three distinct regions: The first is muscle tissue which is predominantly composed of multinucleated myofibers. Myofibers arise through differentiated myotubes, which form by the fusion of multiple myoblasts into multinucleated myotubes with diameters in the range of 20–100 μm . Myofibers are surrounded by a thin layer of connective tissue (endomysium) composed of laminin and collagen type IV.^[29] 20–80 closely parallelly packed myofibers form a fiber bundle.^[30] Several fiber bundles covered by a thin layer of type I collagen-rich perimysium build the matured muscle tissue.^[29] The muscle epimysium (the sheath layer of muscle tissue) primarily consists of large collagen bundles with a crimp pattern reminiscent of that in tendon.^[29] The functionality of skeletal muscle is afforded with contractile fibers or myofibrils.^[30–32] The contracting structures and fundamental units of myofibrils are called sarcomeres.^[31] At the complex interface between cell-rich muscle and ECM-rich tendon, reflecting the second region, the two phases are merged.^[33,34] Tendon, as the third region, is made up of closely packed collagen fibers and sparse fibroblasts.^[34,35]

While skeletal muscle tissues have an inherent ability to regenerate from minor trauma, defects larger than a critical volume ($\geq 20\%$) cannot heal without fibrotic scar tissue formation and partial loss of function.^[30,31,36] Further, repaired tendons are almost always weaker than healthy tendons; this may be due to a lack of mechanical stimulation during the repair stage.^[37] Injuries at the MTJ are common, and failure most likely occurs due to the differences in mechanical properties of muscle and tendon.^[38] Therefore, *in vitro* tissue-engineering approaches are essential to regenerate the anisotropic nature of the MTJ with its complex and highly organized structure.^[39]

Microscopically, MTJ is composed of overlapped fragments of both muscle and tendon tissue and an extensive adhesion surface in between. The ECM, the 3D network of molecules within the tissue, forms a continuum that connects muscle and tendon.^[40] On the side of the skeletal muscle, collagen fibrils provide mechanical

stability and regulate cell adhesion and differentiation.^[40] At the MTJ, muscle fibers form structures that integrate with the ECM elements of the tendon collagen fibers.^[41] The analysis of the mechanisms underlying MTJ formation showed the presence of a unique cluster of cells expressing both myogenic as well as fibroblastic characteristics.^[42] Fibroblasts have switched on a myogenic program, and these dual identity cells fuse into the developing muscle fibers along the MTJs. This mechanism was suggested to result in a hybrid muscle fiber, primarily along with the fiber tips, which enables a smooth transition from muscle fiber characteristics toward tendon features essential for forming robust MTJs.^[42] Additionally, the co-culturing of fibroblasts has been shown to promote the proliferation of C2C12 cells due to the paracrine effect on myoblasts.^[43] The fibroblasts secrete ECM components and growth factors that may also contribute to the improved survival and differentiation of myotubes.^[44] In contrast, in the context of adult wound healing, tendon cells do not regenerate tendons as part of normal healing. Unlike regenerative tissues such as muscle, which are regulated by tissue-specific stem cells that drive tissue replacement, tendons heal by scarring and sometimes by abnormal differentiation toward cartilage or bone.^[40]

Here, we processed a blend of collagen type I/III into continuous non-crosslinked fibers with good mechanical properties and used textile-engineering techniques to fabricate scaffolds supporting contact guidance, alignment, differentiation, and myofiber formation with organized sarcomere structures. We further demonstrated the application of such construct as MTJ model upon co-culture of myoblasts and fibroblasts.

2. Results and Discussion

2.1. Continuous Collagen Fiber Production

Continuous collagen fibers were wet spun, as depicted in **Figure 1**. Collagen I/III grist from equine deep flexor tendon was dissolved in 10 mM hydrochloric acid (HCl) and spun into a coagulation bath containing ammonium hydroxide (NH_4OH) and acetone at a 1:50 volume ratio. Fibers formed upon the pH shift from 3 to 9 and the dehydrating effect of the coagulation bath combined with the shear force (F_S) induced by flowing through the needle (**Figure 1a**).

The protein assemblies obtained in the spinning dope were compared to that obtained in the coagulation bath using atomic force microscopy (AFM) in order to unravel the morphological basis of the continuous fibers (**Figure 1b,c**). In the spinning dope, flat (< 40 nm) and broad (> 10 μm) fibrous agglomerated collagen molecules as well as partially dissolved collagen fibrils (which were likely already crosslinked within the natural starting material), could be identified using cross-sectional analyses (**Figure S1a,b**, Supporting Information), height analyses, and amplitude representations of the AFM scans (**Figure S1c–f**, Supporting Information). In contrast, self-assembled collagen fibrils could be identified in the coagulation bath (**Figure 1c**). The fibril topography indicated a typical D-band pattern with a periodicity of approximately 67 nm, which generally represents a unique ultrastructural feature of all fibril-forming collagens and correlates with the intra-fibrillar register of tropocollagen monomers. The pattern, which is in agreement with the periodicity of native type I collagen observed by Kadler et al.,^[4] has previously not

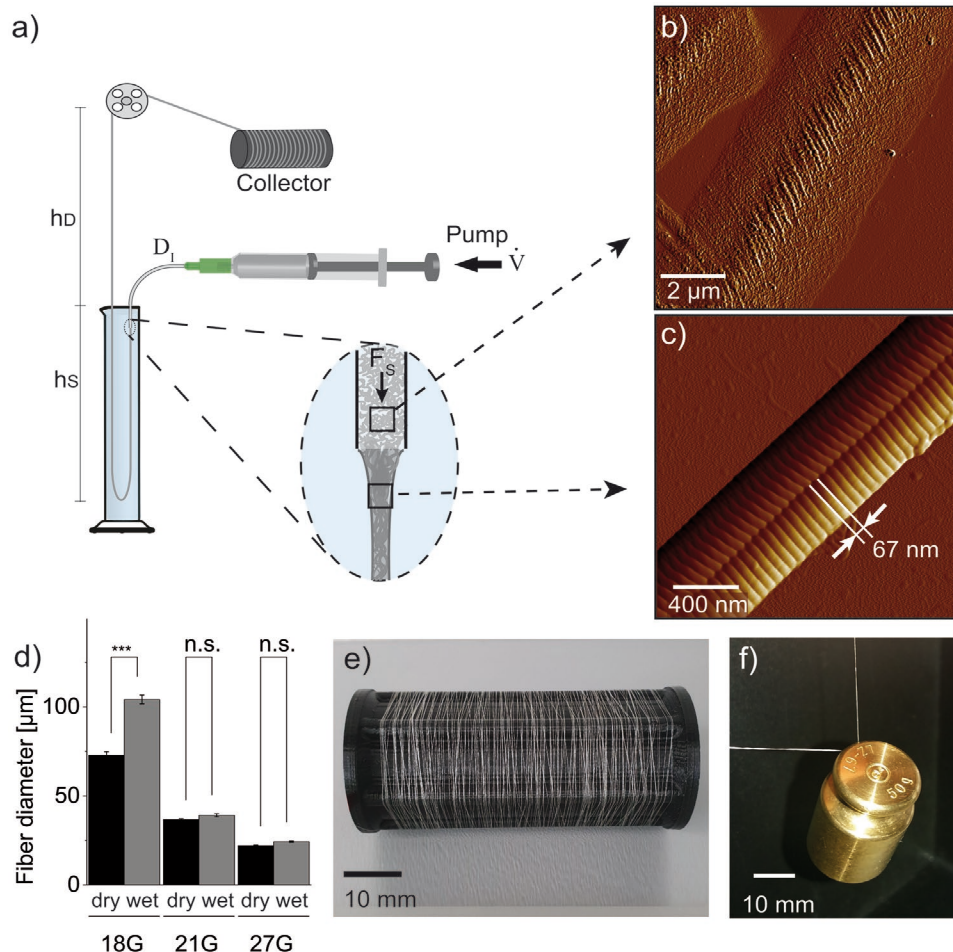


Figure 1. a) Schematic representation of the wet-spinning setup. The collagen solution is extruded into a coagulation bath through a needle connected to a syringe pump. Shear forces (F_s) and a pH shift result in an alignment of the protein chains and fiber formation (close-up). To prolong the exposure time in the coagulation bath, the fibers were spun in a graded cylinder of a specific height (h_s) in order to achieve stable fiber formation and enabling rolling-up. The distance between the coagulation bath and the guide pulley (h_D) and the cylinder height (h_s) were adjusted in accordance with the needle diameter. AFM scans (amplitude representations) of the collagen structures in b) acidic spinning dope and c) in the alkalic coagulation bath. d) Different collagen fiber diameters depending on the needle size in dry and wet state. e) Collagen fibers were collected continuously on a roll. f) A single collagen fiber (\varnothing 80 μ m) is strong enough to lift the load of 50 g.

yet been shown in artificially spun collagen fibers, to the best of the authors knowledge. The results were confirmed in the height images, sectional analysis as well as amplitude representation (Figure S1i–l, Supporting Information). Large area scans and cross-sections thereof (Figure S1g,h, Supporting Information) revealed prevalently well-defined fibrils with diameters of 13–83 nm. The resulting single collagen fibers in different diameters (Figure 1d), spun with a maximal production rate of 34 m h⁻¹ (27G), 25 m h⁻¹ (21G), and 12 m h⁻¹ (18G) were continuously collected (Figure 1e), and a single 18G fiber was strong enough to lift the load of a 50 g weight (Figure 1f).

The flow behavior of collagen type I/III (dissolved in 10 mM HCl) showed decreasing viscosity with increasing shear rate (i.e., a shear-thinning behavior of the solution) due to predominated disentanglement of the collagen molecules, beneficial for the spinning process.^[45] Furthermore, with increasing concentration, the viscosity increased (Figure S2, Supporting Information). The shear rate ($\dot{\gamma}$) during spinning depending on the corresponding volumetric flow rate (\dot{V}) as well as needle diameter influenced

the molecule orientation based on Equation (1).^[46] Higher shear rates resulted in more fibril alignment. The needle gauge (27G) with an inner diameter of 220 μ m and a volume flow rate of 0.4 mm³ s⁻¹ resulted in a shear rate of 392 s⁻¹.

Between 10 and 15 mg mL⁻¹, the wet spinning of collagen was possible, resulting in solid and stable fibers. Fibers were formed with aligned morphology showing strong intermolecular interactions, which is in accordance with observations made by Siriwardane et al. and Zeugolis et al.^[13,21] Concentrations above 15 mg mL⁻¹ yielded in-homogenous fibers, due to less orientation of the collagen fibrils within the fiber.

Mechanically stable fibers were achieved upon extrusion into the coagulation bath to prevent relaxation and reorientation caused by Brownian diffusion.^[47] The height of the coagulation bath and the time in air were dependent on the needle size and the correlating fiber diameter. The thicker the fiber, the more time was needed to solidify and dry the fiber. Spinning with 27G needles required a solidifying height (h_s) of 10–15 cm and a drying height (h_D) of 50 cm.

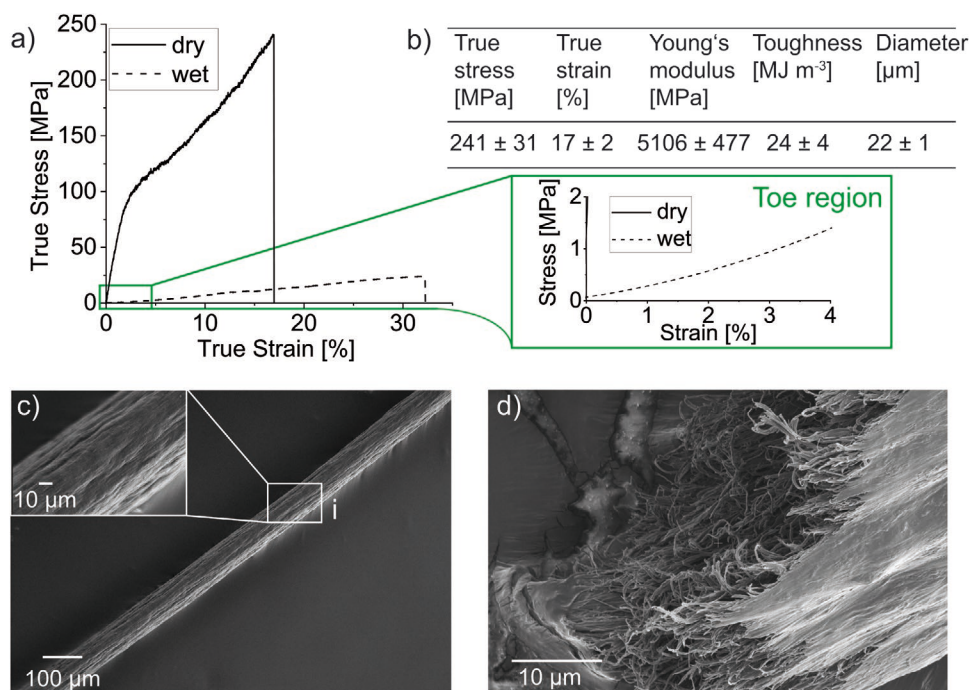


Figure 2. Mechanical and morphological properties of wet spun collagen fibers. a) Representative stress–strain curve of a dry and wet collagen fiber. The inset shows the toe region observed in the case of wet fibers (green box). b) Mechanical properties of wet-spun collagen fibers ($n = 10$). 10 mg mL⁻¹ first dissolved in 10 mM HCl before extrusion into a coagulation bath. c) Representative SEM image of the collagen fiber surface morphology, i) inset showing the grooves on the fiber surface. d) Fracture surface morphology of the breaking point after rupture visualized using SEM showing the collagen fibrils.

2.2. Fiber Characterization

In the stress–strain curves of collagen fibers (Figure 2a), dry fibers showed a linear elastic region from 0% to 2% strain followed by a viscoelastic deformation until a breakpoint at around 16% strain. In wet state, the stress–strain curve of the collagen fibers showed a toe region (0–5%) at the beginning (Figure 2a, enlargement), followed by an elastic region with fiber failure at the end.

Calculated toughness and tensile strength of collagen fibers were indistinguishable independent of the solvent used using a 10 mg mL⁻¹ spinning dope. Only the Young's modulus (5106 ± 477 MPa) obtained for fibers spun out of HCl was slightly higher compared to that of fibers spun out of acetic acid (AcOH) (4089 ± 472 MPa) (Table S1, Supporting Information).

When hydrated, the collagen fibers generally showed lower tensile strength, Young's modulus, and toughness but higher elongation and diameter than dry-state fibers (Table S2, Supporting Information).

Our values of 241 MPa were comparable to that of fibers produced by Siriwardane et al.^[13] (240 MPa) and Zeugolis et al.^[21] (237 MPa). The tensile strength was slightly lower despite not being crosslinked in comparison to fibers made by Haynl et al.^[17] (383 MPa). The higher values are probably due to the lower fiber diameter in that study, in which microfluidic channels were used for collagen spinning. The Young's modulus of the collagen fibers prepared here (5106 ± 477 MPa) showed significantly higher values than that of all previously published fibers.

The air-dried fibers appeared homogeneous with a slightly rough surface (Figure 2c) and a nanofibrillar sub-structure

(Figure 2d). The scanning electron microscope (SEM) micrograph (Figure 2d) confirmed the AFM data (Figure 1; Figure S1, Supporting Information), showing the implementation of the fibrils into the core structure of the final collagen fibers. Such structures resemble the hierarchical setup of high-performance protein fibers such as silk fibers.^[48,49] The sub-structures significantly contribute to the mechanical performance by homogeneously distributing the pulling stress.^[48,49] Overall, these results show a straight forward fabrication technique for continuous collagen fiber production without any crosslinking. The tunable mechanical properties of the reported fibers predestinate them for the formation of anisotropic tissues.

2.3. Cell-Fiber Interaction

As skeletal muscle tissue consists of muscle fiber bundles formed after the fusion of undifferentiated myoblasts into multinucleated, long, and cylindrical myotubes, the fiber matrix likely plays an important role in guiding the formation of muscle bundles.^[50]

First, we evaluated the proliferation, viability, and alignment of C2C12 mouse myoblasts on our collagen fibers with that on treated tissue culture plates (TCP) or collagen films as controls (Figure 3). Live-dead assays showed cell viability above 90% on collagen fibers and films after 1, 3, and 7 days of culture (Figure S3a,b, Supporting Information). No significant differences were detected between the viability of the cells cultured on fibers with different diameters and films. However, it has to be mentioned that live-dead assay results are limited,

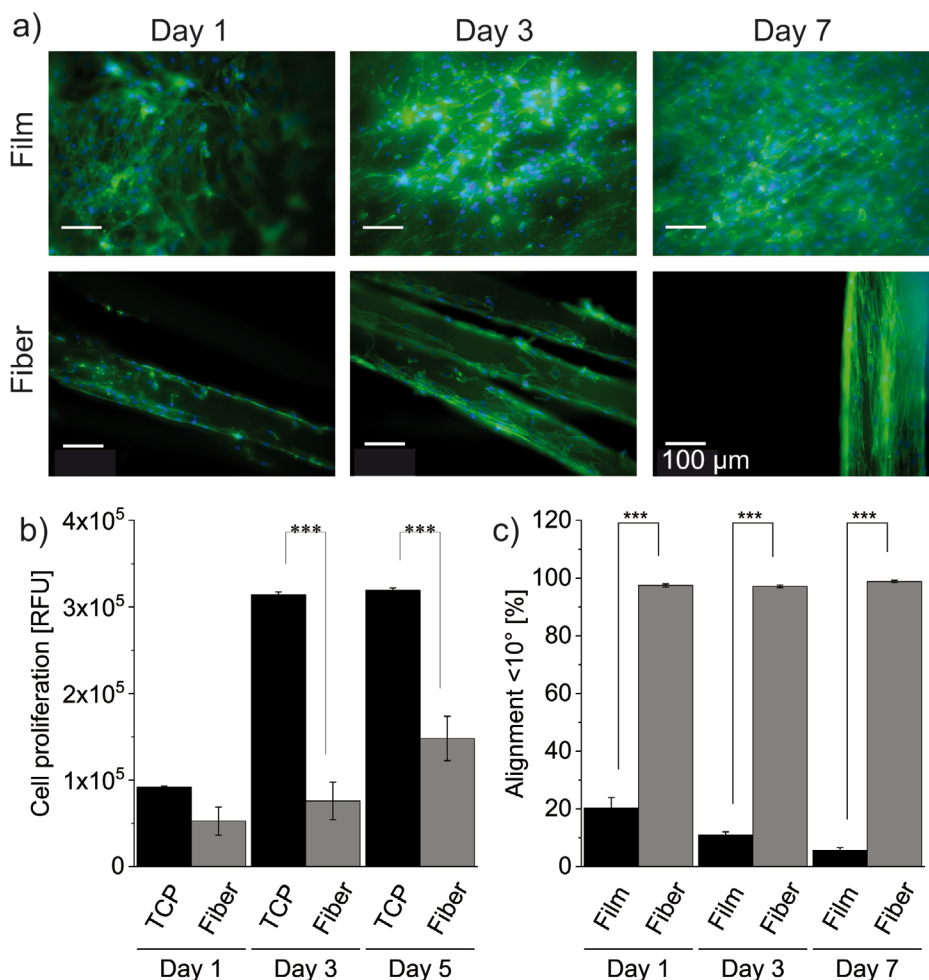


Figure 3. Cell culture analysis of C2C12 myoblasts on collagen films, or wet spun collagen fibers. a) Cell alignment: Fluorescence images of 4',6-diamidino-2-phenylindole dihydrochloride (DAPI) (blue, nuclei)- and phalloidin (green, actin filaments)-stained cells after 1, 3, and 7 days of cultivation. b) AlamarBlue proliferation assay of cells on TCP (acting as positive control) or collagen fibers after 1, 3, and 5 days showing an increased metabolic activity. c) Quantification of cell alignment on collagen fibers or collagen films (cell body orientation angles of $<10^\circ$ to fibers were considered as aligned) ($n = 3$; significant differences: $***p \leq 0.001$). Scale bars are 100 μm .

as dead cells usually detach from surfaces and would not be visible. The additionally performed alamarBlue assay clearly showed proliferation and an increasing number of living cells on TCP and fibers through increased metabolic activity after 3 and 5 days (Figure 3b). The cells perfectly aligned on collagen fibers in contrast to the random orientation and spread morphology on collagen films. Cell orientation and alignment were visualized and quantified using fluorescence images after staining actin filaments (Figure 3a,c). The quantitative analysis revealed cell bodies' alignment on fibers on day 1 and 7, with $98 \pm 1\%$ and $99 \pm 1\%$, respectively. In contrast, cell alignment on collagen films decreased from $20 \pm 4\%$ on day 1 to $6 \pm 1\%$ on day 7 (Figure 3c). Furthermore, the oriented cells grown on fibers and films were imaged after 1 day using SEM (Figure S3c,d, Supporting Information). C2C12 cells on fibers spread along the fiber axis and showed a highly aligned morphology. The fiber surface perfectly guided the cell's contact and adhesion, showing an aligned morphology along the fiber axis.

2.4. Myogenesis on Collagen Fibers

To investigate the differentiation of myoblasts into myotubes, differentiation was induced after 9 days of culture and continued for 7 days. Figure 4 shows the positive effect of fiber morphology on myogenesis compared to that of the control (TCP). For quantification, a minimum of 5 images and 50 myotubes were analyzed per setting. After 7 days, the majority of C2C12 myoblasts had fused and formed multinucleated myotubes along the collagen fiber axis with a maximum length of 600 μm (Figure 4c,h). Myotubes formed on collagen fibers showed well-formed A bands and Z-lines (Figure 4e,f) visible at the borders as well as in the center of the myotubes. Myotubes on collagen fibers were well aligned (96%) (Figure 4g). The average length of myotubes formed on TCP, after 7 days of differentiation, was higher ($\approx 640 \mu\text{m}$) than on fibers ($\approx 380 \mu\text{m}$), which is due to the larger area for the access of cells on the tissue culture plate (12-well plate) (Figure 4h). However, the aspect

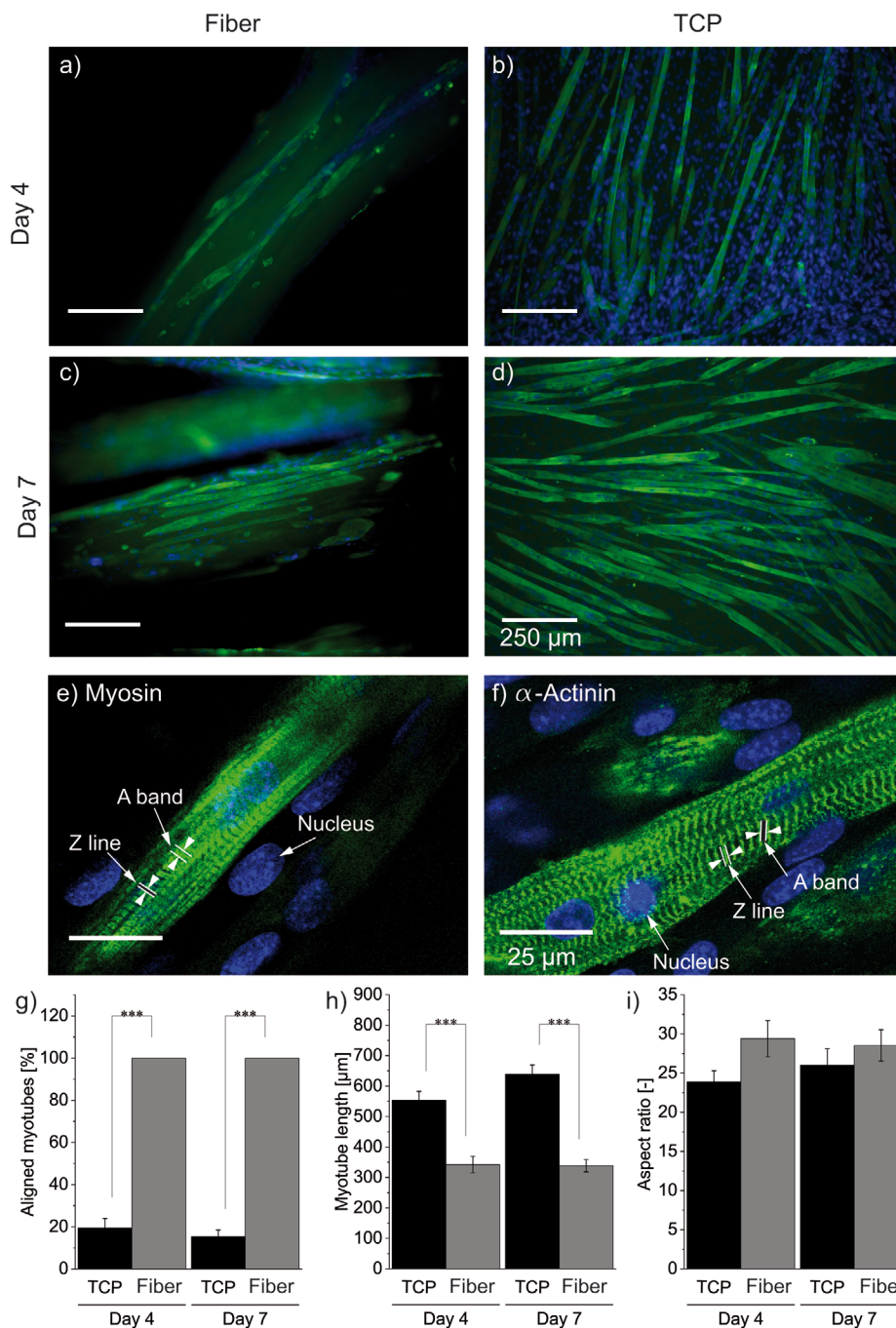


Figure 4. Myogenesis of C2C12 myoblasts on wet spun collagen fibers. a–d) Fluorescence images of cells cultured on TCP or collagen fibers after 4 and 7 days of differentiation (stained with mouse anti-fast skeletal myosin antibody, using Alexa Fluor 488 conjugated IgG secondary antibody and Hoechst to stain nuclei). Scale bars are 250 μm . e, f) Fluorescence confocal images showing the myotubes' internal structure after staining using mouse anti-fast skeletal myosin antibody or anti-sarcomere α -actinin antibody and Alexa fluor 488 conjugated IgG as a secondary antibody showing nuclei, A bands and Z lines (indicated by arrows). Scale bars are 25 μm . g) Alignment of myotubes (cell body orientation angles of $<10^\circ$ to fibers were considered as aligned), h) myotube length, and i) aspect ratio (myotube length/width) formed on wet spun collagen fibers or TCP after 4 and 7 days in differentiation medium ($n = 3$; significant differences: $**p \leq 0.01$, and $***p \leq 0.001$).

ratio of the myotubes on TCP was lower, which was due to the larger width of the formed myotubes on TCP (Day 4: 24 ± 2 , Day 7: 26 ± 2) compared to myotubes formed on collagen fibers (Day 4: 27 ± 2 , Day 7: 27 ± 2) (Figure 4i).

The contractile activity of the skeletal muscle cells depends on the precise spatial arrangement of myofibrils in myotubes.^[51] Repeated units in the structure of myofibrils, known as sarcomeres, consist of myosin (thick filament) and actin (thin

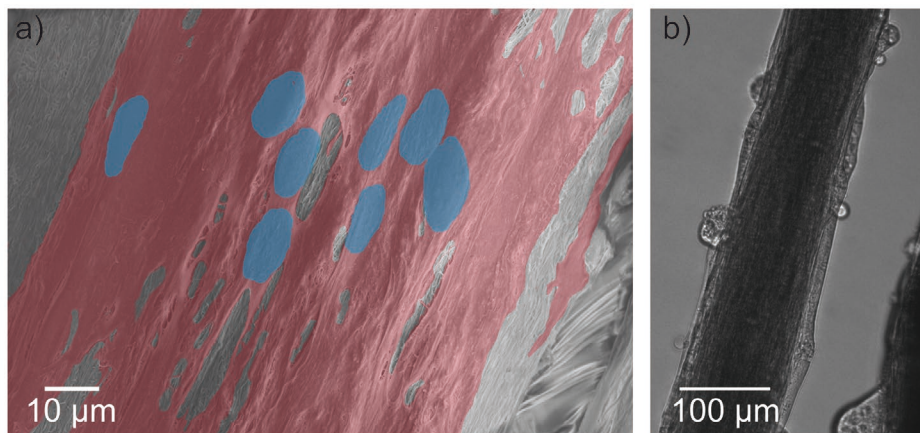


Figure 5. Representative images of multinucleated myofibers. a) SEM image of myotubes (cell body false colored in red, cell nuclei colored in blue) on a collagen fiber after 7 days of differentiation. Cells grew and fused along the fiber axis. b) Light microscopy image of myotubes on collagen fibers during electrical stimulation (length \approx 650 μm).

filament) arranged in a repetitive manner.^[52] The repeated units are visible under the microscope as two dark lines originating from densely packed proteins (Z lines) between which two light bands of actin filaments (I bands) are located. I bands are separated by a dark A band containing myosin filaments.^[53] Due to the critical role of myofibril assembly in muscle contraction, immunostaining toward myosin and α -actinin was performed to visualize the A band and Z line (Figure 4e,f). Next, the contractibility of the myofibers was tested after stimulation with electrical pulses. A synchronous contraction could be observed in differentiated myotubes after electrical stimulation (using 3–6 V, frequency: 1 Hz, duration: 1 ms), further confirming the intracellular organization of sarcomeres and myofiber maturation (Figure 5; Movie S1, Supporting Information). The myofibers started beating synchronously after applying continuous square electrical pulses (Movie S1, Supporting Information). Altogether, our results clearly showed contraction and formation of A bands and Z lines in the majority of the myotubes, confirming the suitability of the collagen fibers to support the

formation of myofibers with a regular array of sarcomeres and striated morphology similar to that of natural skeletal muscle fibers.^[54]

2.5. Processing of Collagen Fibers into Complex Structures

Next, we evaluated textile-engineering techniques such as weaving and braiding to process the wet spun collagen fibers, extending their applicability to more complex 3D structures (Figure 6). Using a 3D printed tape loom (Figure 6a) with 21 warp and one weft threads, flat structures (2D) with widths of 1200 μm (21G fibers, Figure 6b) and 1700 μm (18G fibers) and tubular woven structures (3D) with an inner diameter of 500 μm (21G fibers, Figure 6c) and 1000 μm (18G fibers) were created. Using a 3D printed frame, another flat structure was fabricated by weaving 21G collagen fibers into a $3 \times 3 \text{ cm}^2$ construct (Figure 6d). By braiding three single collagen fibers, an 8 cm-long, flat, solid, three-stranded structure was fabricated (Figure 6e).

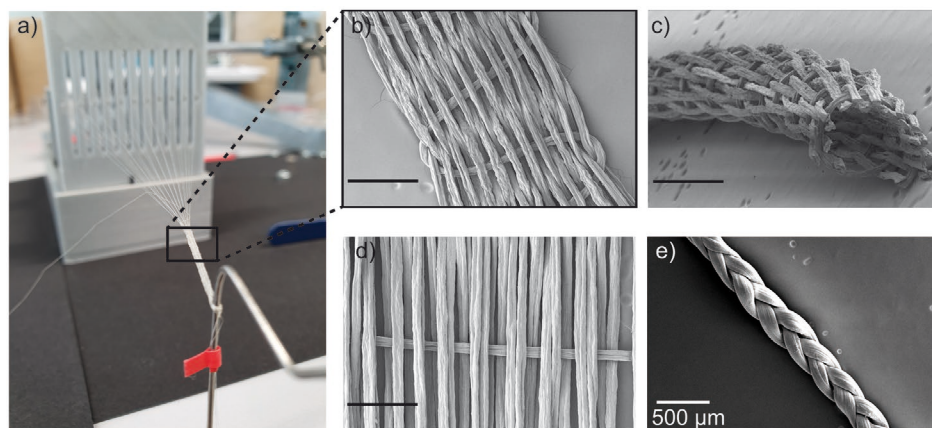


Figure 6. Collagen fiber processing. a) Photograph of the tape loom used to fabricate flat and tubular woven collagen structures. SEM images of structures with various morphological features fabricated using wet spun collagen fibers. Image of collagen fibers woven in a b) flat and c) tubular structure fabricated using a tape loom. d) Image of a flat structure created by weaving collagen fibers using a frame. e) Image of a braided structure using three single collagen fibers. Scale bars are 500 μm .

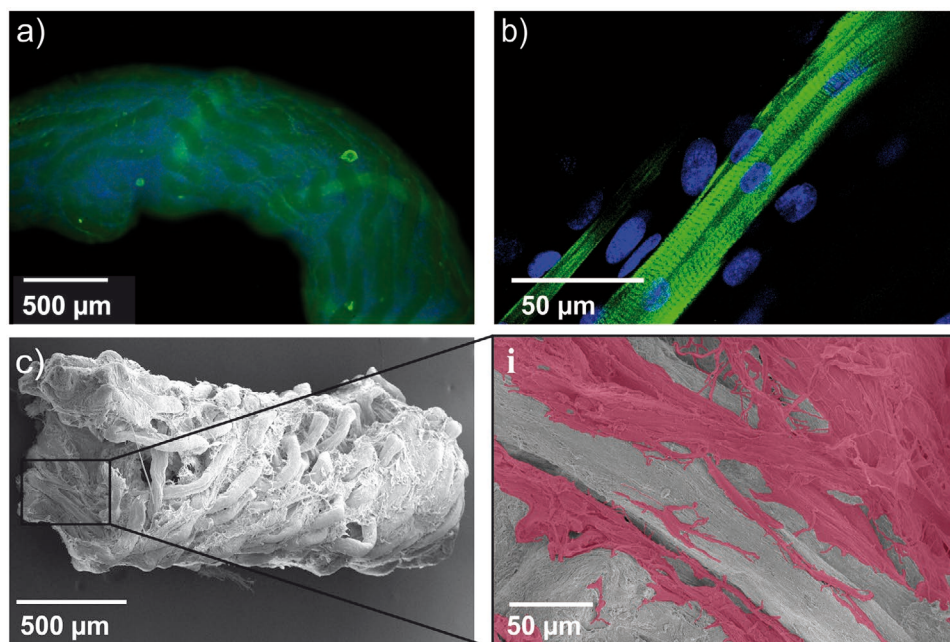


Figure 7. 3D woven tubular structures based on our wet spun collagen fibers. a) Fluorescence image of C2C12 myofibers cultured on a collagen fiber tube after 7 days of culture (stained with anti-sarcomeric α -actinin antibody, revealed by Alexa fluor 488 conjugated IgG secondary antibody and Hoechst to stain nuclei). b) Fluorescence confocal image of a C2C12 myotube and its sarcomere structure (stained with mouse anti-fast skeletal myosin antibody, revealed by Alexa fluor 488 conjugated IgG secondary antibody and Hoechst to stain nuclei) on a collagen fiber tube after 7 days of differentiation. c) SEM image of multinucleated myotubes on a collagen fiber tube after 7 days of differentiation and a i) close-up image showing myotubes covering the tube surface (cell body colored in red).

To the best of our knowledge, only one report from Tonndorf et al. exists on pure assembled collagen structures made from wet-spun collagen multifilament yarns (comprising 6 filaments).^[11] However, the single collagen fibers used there showed an irregular cross-section, only flat structures were produced, and they were relatively large due to the assembly of the 6-filaments yarn. Similarly, Xie et al. created collagen/Poly lactic acid (PLA) scaffolds using a knitting machine for a potential cardiac application.^[55] However, they were not able to produce pure collagen scaffolds, and processed structures were only flat.

2.6. Myogenesis on Collagen Fiber Structures

Textile engineering approaches have been previously used in musculoskeletal tissue engineering to fabricate substrates with specific morphology and strength for the functional repair of ligaments and tendons, but to the best of our knowledge, these structures were not fabricated to produce anisotropic scaffolds for skeletal muscle tissue engineering.^[27,28,56] As wet spun collagen fibers provided excellent support for C2C12 myogenesis and the formation of long, aligned, and multinucleated myofibers along the fiber axis (Figure 4), two different morphologies were chosen to analyze the formation of muscle microtissue. Tubular woven structures (Figure 6c) and flat structures (Figure 6b) made from 21G or 18G wet spun collagen fibers were seeded with C2C12 myoblasts. After 6 days of culture in growth medium, differentiation of myoblasts into myotubes was induced and continued for another 7 days.

Fluorescence (Figure 7a) and SEM (Figure 7c) imaging of myotubes formed on collagen fiber assemblies showed high

alignment of myotubes along the fibers, covering the entire tube surface (Figure 7c,i cell body colored in red). Tubular constructs were first imaged on the fiber surface and afterward cut lengthwise to image the internal cross-section. The open spaces between the fibers allowed the cells to spread inside and outside. Moreover, the open pores facilitated nutrition and waste product exchange within the tubular ($6857 \pm 3897 \mu\text{m}$) and flat ($7173 \pm 2384 \mu\text{m}$) assemblies. Both flat and tubular collagen fiber structures were completely covered with myotubes inside and outside. Furthermore, immunofluorescence imaging of stained myotubes using confocal microscopy (Figure 7b) clearly showed the multinuclear structure and presence of sarcomere myosin in differentiated myotubes formed on the collagen fiber assemblies. Therefore, it can be concluded that the produced 3D constructs can support muscle fiber formation with an organized internal structure similar to that of native tissue.^[30,57]

2.7. Co-Culture of C2C12 Myoblasts and NIH/3T3 Fibroblasts to Develop an MTJ Model Using Collagen Fiber Assemblies

To mimic the MTJ situation (Figure 6a), we co-cultivated C2C12 myoblasts and NIH/3T3 fibroblasts on flat structures made from 21G wet spun collagen fibers shown in Figure 6b. In a first approach, both C2C12 myoblasts and NIH/3T3 fibroblasts were labeled with cell tracker, C2C12 with green and fibroblasts with red stains (see experimental section for details).

Successful adhesion and proliferation of both cell types were demonstrated on our collagen fiber-based constructs. Both cell types grew along the fiber surface and proliferated within five days of culture (Figure 8c). Then, they were moved to the

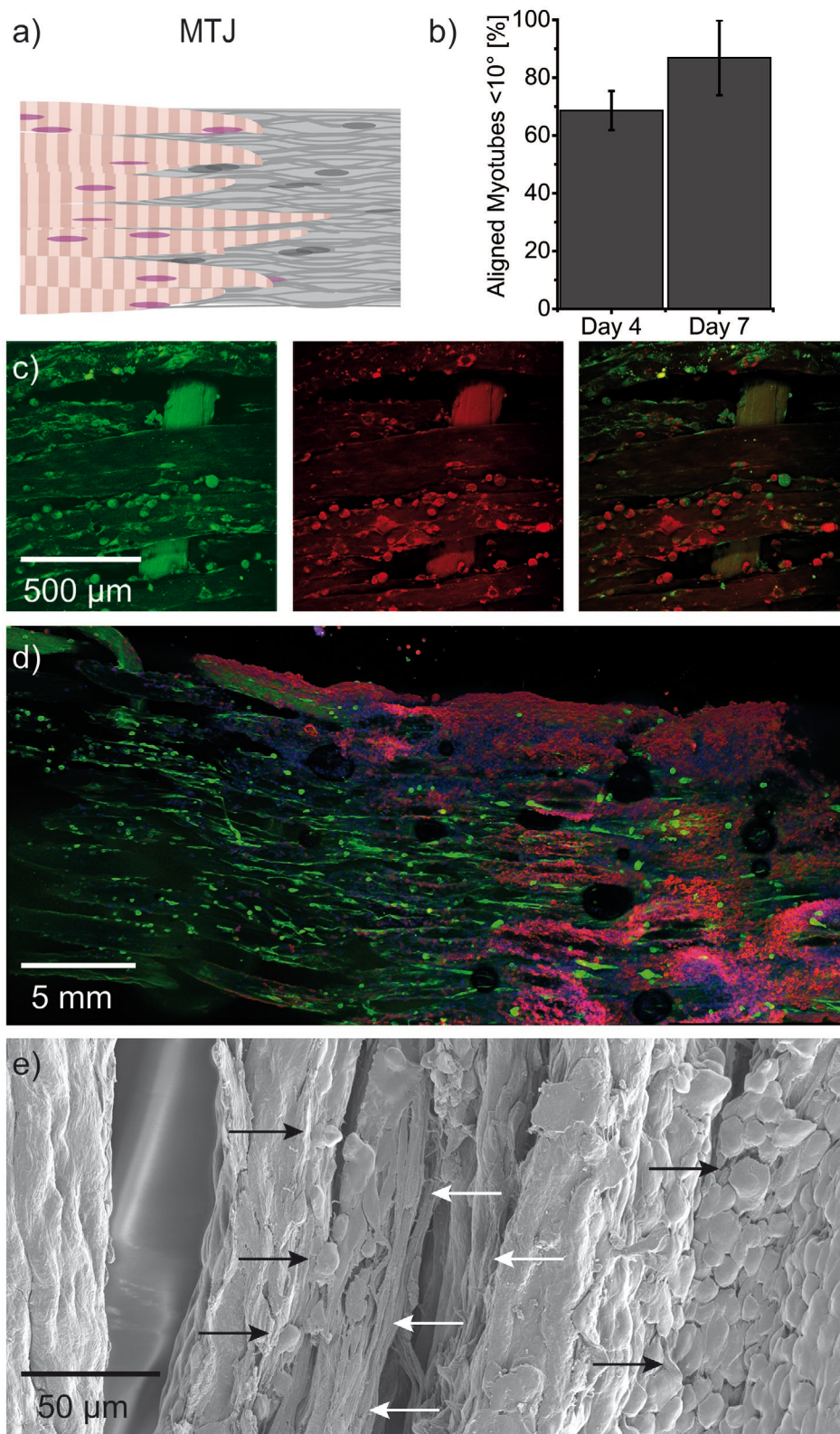


Figure 8. Co-culture of C2C12 myoblasts and NIH/3T3 fibroblasts on flat collagen fiber structures. a) Schematic illustration of MTJ tissue. b) Alignment of myotubes formed on collagen fiber constructs after 4 and 7 days in differentiation medium (cell body orientation angles of $<10^\circ$ to fibers were considered as aligned). c) Confocal images of C2C12 (green) and fibroblasts (red) stained using cell tracker (see Experimental Section for details) after 3 days of cultivation in growth medium. d) Confocal image of C2C12 myotubes (α -actinin, green) and fibroblasts (actin, red) after 7 days of differentiation. e) Representative SEM image of co-cultured C2C12 (white arrows) and fibroblasts (black arrows) after 7 days of differentiation on our collagen structures.

differentiation medium. Formation of long and aligned myotubes after changing to differentiation medium was visible in samples cultured with labeled cells. Cells which were labeled with cell tracker were still visible, and myotubes formed after the fusion of the labeled cells appeared green within the red labeled fibroblast cells after almost ten days of culture.

In a second approach, cells were seeded on the constructs like in the previous approach but without cell tracker. After five days of culture in the growth medium, the cell constructs were moved to the differentiation medium for another seven days. After day 7, nuclei were stained with Hoechst, and cells were immunostained using anti-sarcomere α -actinin (green color) for myotubes and actin (red color) staining for fibroblasts. Using confocal microscopy (Figure 8d) and SEM (Figure 8e), fibroblasts (black arrows) and myotubes (white arrows) were detected on the collagen fiber assemblies. After seven days of culture, highly aligned myotubes ($87 \pm 13\%$, Figure 8b) are perfectly visible on the left side of the constructs and fibroblasts on the right side of the construct, covering the entire structure surface. Furthermore, myotubes were not only formed on the surface but also in deeper levels within the constructs (Figure S5 and Movie S2, Supporting Information). Therefore, it can be concluded that the co-culture of fibroblasts and myoblasts on 3D fabricated collagen constructs can be used as a model for the MTJ.

3. Conclusion

Wet-spun collagen I/III microfibers were produced with an internal fibrillar structure showing a D-band pattern typical for native collagen fibers. By processing these mechanically stable collagen microfibers using textile engineering techniques, more complex 3D-constructs with inter-porosities were achieved. Collagen-based tubular and flat structures are beneficial for designing skeletal muscle microtissues because they enable the formation of long, aligned, and contractile myofibers. The generated 3D muscle fiber bundles showed highly organized intracellular organization and synchronous contraction after electrical stimulation, confirming the mature state of the myofibers. Further, an MTJ model was established using a co-culture of C2C12 and NIH/3T3 fibroblasts with both cell types growing and proliferating along the collagen fibers. This approach is well suited to allow the gradual fabrication of functional tissue in vitro, which can be used to mimic the native MTJ structure for further applications. Overall, the significance of these collagen-based assemblies based on non-crosslinked collagen fibers with tubular structures can expand into the fabrication of vascularized and innervated tissue for several biomedical applications.

4. Experimental Section

Materials: Collagen I/III grist from equine deep flexor tendon was provided by RESORBA (Nuremberg, Germany). Ammonium hydroxide (NH_4OH), Phalloidin-Tetramethylrhodamin B-Isocyanate from Amanita phalloides, and tert-butanol were purchased from Sigma-Aldrich (Taufkirchen, Germany). Acetic acid (AcOH), Acetone, Dulbecco's modified Eagle's medium (DMEM), fetal bovine serum

(FBS), pure ethanol, hydrochloric acid (HCl), and phosphate buffered saline (PBS) were obtained from VWR (Darmstadt, Germany). Treated well plates, Phalloidin Dylight 488, DAPI, penicillin/streptomycin (pen/strep), goat anti-mouse IgG-Alexa Fluor 488 (A11001), glutamine, Hoechst 33258, Insulin-Transferrin-Selenium Supplement (100 \times) (ITS), minimum essential medium (MEM), MEM-essential amino acid, SYTO Green Fluorescent Nucleic Acid Stain Sampler Kit, and treated as well as non-adherent well plates were obtained from Thermo Fisher Scientific (Bonn, Germany). Mouse monoclonal anti-fast skeletal myosin IgG antibody (MY-32, ab-7784) and anti-sarcomere α -actinin antibody (EA-53, ab-9465) were obtained from Abcam (Cambridge, UK). Cell tracker red CMTX was purchased from Invitrogen. All other chemicals were purchased from Carl-Roth GmbH + Co KG (Karlsruhe, Germany).

Preparation of Wet Spinning Solutions: Collagen I/III grist was dissolved in either AcOH (350 mM) or HCl (10 mM) at different concentrations (5, 10, and 15 mg mL^{-1}) to achieve homogeneous solutions. The mixture was shaken vigorously until no pieces were visible, and mixing was continued for two days at 4 $^{\circ}\text{C}$. Next, it was filtered through a membrane (90 \times 90 μm mesh) and centrifuged at 10 000 \times g for 10 min to remove air bubbles.

Wet Spinning: Collagen solutions were extruded into a coagulation bath consisting of NH_4OH and acetone at a 1:50 v/v ratio (pH 9) using a syringe pump (Harvard Apparatus Inc., Holliston, MA, USA) using flow rates of 25–30 $\mu\text{L min}^{-1}$ (27G), 45–50 $\mu\text{L min}^{-1}$ (21G), and 70–75 $\mu\text{L min}^{-1}$ (18G). Solid fibers were air-dried and guided over a guide pulley to the collecting drum and automatically collected.

Collagen Film Production: Collagen films were prepared by casting collagen solution (10 mg mL^{-1}) into a 35 mm glass dish followed by adding coagulation solution and overnight incubation in a closed dish. Afterward, films were washed with water and dried overnight.

Fiber Processing: Collagen fibers were woven into flat and tubular structures using a 3D printed tape loom. One continuous collagen fiber was wound through the holes and slots of the heddle as warp threads (21 threads), and fibers were fixed about 10 cm in front of the heddle (Figure S4d, Supporting Information). One weft collagen fiber was then wound around a shuttle, and the end was fixed to the warp threads. For weaving, warp threads were moved up and down while the weft thread was passed through the alternating shed.

AFM Analysis: Collagen solution (0.1 mg mL^{-1} , 40 μL) was spotted on freshly cleaved mica plates (ϕ 10 mm, V1 grade, Plano GmbH, Germany) and incubated for 5 min. One sample was washed with MilliQ water, and one sample was treated with wet spinning coagulation buffer for 5 min before washing.

AFM imaging of dry nanofilm samples was performed on a Dimension ICON with Nano scope V controller (Bruker, Santa Barbara, CA) in Tapping Mode using Si cantilevers (OTESPA-R3, f_0 300 kHz, k : 26 N m^{-1} , Bruker). For imaging, light tapping (ratio of set point amplitude to free amplitude ≈ 0.7 – 0.9) was applied. AFM scans were processed using Nano Scope Analysis Software Version 1.50 (Bruker, Santa Barbara, CA).

Rheological Analysis: The viscosity of the collagen solutions was analyzed using a shear rheometer (Discovery HR-2, TA Instruments, Eschborn, Germany) in rotation mode with a 25 mm steel plate geometry and a gap size of 100 μm . A ramp test was performed with a shear rate range of 1–1000 s^{-1} and a measuring time of 4 min at 25 $^{\circ}\text{C}$. These measurements were repeated on five individual samples from each experimental group. The approximated shear rate within the used needles was calculated depending on the corresponding volume flow rate using the equation Hagen/Poiseuille:^[45]

$$\dot{\gamma} = \frac{4 \cdot \dot{V}}{\pi \cdot R^3} \quad (1)$$

where $\dot{\gamma}$ is the shear rate, \dot{V} the volumetric flow rate and R the radius of the needle.

Tensile testing: Mechanical properties of the fibers were determined using a tensile testing device (ElectroForce 3200, TA Instruments, DE, USA) with 2.5 N or 0.49 N load cells for testing dry and wet fibers, respectively. Small sections of collagen fibers were randomly selected

and fixed onto paper frames with a gap of 10 mm using two-component glue in case of dry samples. The glue was left to dry under a fume hood for at least 12 h. For tensile testing in wet condition, one layer of a PLA (black PLA filament, Ultimaker 3, Germany) frame was 3D printed using an Ultimaker 3 (Ultimaker, Germany), then fibers were placed on the first layer in the middle of the frame, and a second layer was printed on top. Before testing, fibers were incubated in MilliQ water for 48 h. Fiber diameters were measured using a light microscope. The frames were then fixed between the clamps of the testing device and pulled apart until failure at a rate of 0.01 mm s^{-1} at a relative humidity of 40%, and room temperature (RT). The Young's modulus (E) was obtained by calculating the slope of the stress–strain curve in the linear elastic region. The fiber toughness was calculated by integrating the stress–strain curve. The measurements were repeated for a minimum of ten individual samples.

Cell Culture Experiments: Collagen fibers were incubated with murine C2C12 muscle cells (ATCC CRL-1772, Manassas, VA). Six pieces of collagen fibers with different diameters were fixed in CellCrown inserts (Scaffdex, Finland). After multiple washing steps with water and 70% ethanol for one hour, fibers were moved to Dulbecco's phosphate-buffered saline (DPBS), washed with PBS, and sterilized on a clean bench with UV light for 20 min. C2C12 cells were trypsinized and cultured on fibers, films, or TCP. After 30 min incubation of cell suspension with samples at 37°C , a growth medium was added to each sample and was refreshed every two days. The growth medium of C2C12 cells contained DMEM, FBS (10% v/v), penicillin/streptomycin (1% v/v), glutamine (4 mM), and 4-(2-hydroxyethyl)-1-piperazineethanesulfonic acid (20 mM).

The proliferation rate was measured using the alamarBlue assay after culturing 10 000 cells per well on fibers and TCP after 1, 3, and 5 days of culture. According to the manufacturer's protocol, reagent (10%) was added to the samples at each time point, incubated for 90 min at 37°C and stirred gently every 30 min to avoid gradients. The reacted media was removed from each sample and kept on ice in the dark; the solution (100 μL) was transferred to a 96-well plate followed by measuring its absorbance using a plate reader (Mithras LB, Germany) at 560 nm (excitation) and 590 nm (emission) wavelength. The negative control was prepared by mixing 10% alamarBlue in medium. Three repeats were performed for each experiment.

For live/dead staining and cell alignment, 1.2×10^6 cells mL^{-1} were cultured on fibers or films. To study myogenesis, 1×10^5 cells mL^{-1} were cultured on fibers or tissue culture plates. Live dead staining: Viability and proliferation of C2C12 cells were evaluated on the collagen fibers after 1, 3, and 7 days of culture in growth medium. Three repeats per sample were stained and imaged using fluorescence microscopy (Leica DMI8, Germany). Cells were stained following the manufacturer's protocol (Thermo Fisher Scientific (Bonn, Germany) upon addition of ethidium homodimer-1 (dead cells) and calcein (live cells). The viability was measured by analyzing five images per sample and by dividing the counted live cells by the total number of cells.

Cell alignment: Cell elongation and cell alignment were evaluated after 1, 3, and 7 days of culture in growth medium by staining actin filaments and nuclei using Phalloidin and DAPI. To stain the actin filaments and nuclei after fixation of samples using 3.7% formaldehyde, cells were permeabilized using Triton (0.1% v/v) for 5 min at RT. The staining solutions, DAPI and phalloidin were added to the samples followed by 30 min incubation at RT. Fluorescent microscopy was used for imaging the cells, and 5 images of each sample were further analyzed with Image J to investigate cell alignment. Cell bodies showing orientation angles less than 10° were considered as aligned.

The same samples were also used to analyze the morphology of the cells and fibers using SEM (Carl Zeiss Microscopy GmbH, Germany, and Apreo VS, Thermo Fisher Scientific, Germany). Therefore, the samples were dehydrated using a gradual concentration of ethanol in water (50%, 70%, 80%, 90%, 100%) on ice for 5 min. Samples were completely dehydrated using a 1:2 dilution of tert-butanol in ethanol and pure tert-butanol for 5 min at RT, and frozen at -80°C for 1 h before lyophilization overnight. Before imaging using SEM, samples were sputter-coated for 30 s at 30 mA with gold.

Myogenesis on Collagen Fibers: After 9 days of culture on collagen fibers and TCP, myoblasts were moved to differentiation medium and cultured for 7 days. The composition of the differentiation medium was similar to that of the growth medium, but additionally contained horse serum (2%). The differentiation medium was refreshed every 3 days. The formation of myotubes was visualized after 4 and 7 days. Cells were fixed with formaldehyde (3.7% v/v) in DPBS for 15 min at RT, permeabilized with Triton X-100 (0.3% v/v) for 5 min at RT, blocked with glycine (300 mM) for 30 min at RT, again blocked with bovine serum albumin (BSA) (5% w/v) in DPBS for 20 min at RT, and incubated with mouse monoclonal anti-fast skeletal myosin IgG antibody diluted 1:1000 in DPBS containing BSA (0.1% w/v) overnight at 4°C . The samples were then incubated for 60 min with the goat anti-mouse IgG-Alexa Fluor and Hoechst at a 1:1000 dilution in BSA (0.1% w/v). Random images were captured using a fluorescence microscope to evaluate myotube length, width, alignment, and aspect ratio.

Electrical Stimulation of Myotubes on Collagen Fibers: Differentiation of C2C12 cells cultured on collagen fibers was induced after 11 days of culture in growth medium and was continued for 7 days in differentiation medium. The formation of myotubes was visualized, and on day 7 after differentiation, cells were stimulated electrically using a custom-made electrical stimulation device to evaluate the functionality of the myotubes. Collagen fibers were moved to stimulation medium (differentiation medium + MEM-non-essential amino acid + MEM-essential amino acid (2% v/v)). For stimulation, following the authors' previous studies,^[58] the electrical field was applied to two parallel platinum wires attached to the dish cap with a separation of 1.5 cm placed perpendicular to the collagen fiber axis in a 35 mm culture dish. Myotubes were stimulated without any training by applying an electrical square-wave pulse (6 V, frequency: 1 Hz, duration: 1 ms). Time-lapse imaging was performed to image the beating myotubes (Leica DMI8, Germany).

Myogenesis on Collagen Fiber Assemblies: Collagen fiber structures were prepared as described before. After multiple washing steps with water and 70% ethanol for 1 h, collagen fiber assemblies were sterilized on a clean bench using a UV light for 20 min. In flat woven samples, growth medium was added to each sample after seeding cells on top and incubating for 1 h at 37°C . In tubular structures, cells were pipetted into the opening and incubated for 1 h at 37°C at 1 rpm using a rotational mixer. After 1 h, tubes were transferred to an ultra-non-adherent well plate, and growth medium was added. After 6 days of culture in the growth medium, samples were transferred to the differentiation medium and incubated for another 7 days. The composition of the differentiation medium was similar to the previous experiment, and additional ITS (1% v/v) was added. The differentiation medium was changed every 3 days.

The formation of myotubes and the sarcomere structure was visualized after 7 days of differentiation. Cells were fixed, permeabilized, blocked, and either incubated with mouse monoclonal anti-fast skeletal myosin IgG antibody diluted 1:1000 in BSA (0.1% w/v) solution or with anti-sarcomere α -actinin antibody diluted 1:200 in BSA (0.1% w/v) solution at 4°C overnight. The samples were then incubated for 60 min with the goat anti-mouse IgG-Alexa fluor 488 1:200 and Hoechst, at a dilution of either 1:1000 (myosin staining) or 1:200 (α -actinin staining) in BSA (0.1% w/v) solution. Random images were taken using a fluorescence microscope and confocal microscope (Leica DMI8 SP8 HyVolution, Germany) to evaluate myotube formation.

Co-Culture Experiments: Collagen fibers were prepared and sterilized as before. Two groups of samples were prepared. In the first approach, both, C2C12 myoblasts and NIH/3T3 fibroblasts, were labeled with two different cell trackers before cultivation. Cell tracker red CMTPX was used to label NIH/3T3 fibroblasts, and the SYTO 9 green cell tracker was used to label C2C12 mouse myoblasts. According to the manufacturer protocols, 100 000 cells mL^{-1} were incubated in a medium containing CMTPX (5 μM) (fibroblasts) or SYTO (10 nM) (C2C12) for 1 h at 37°C . Small volumes containing (10 μL) 100 000 cells of each cell type were carefully cultured on each side of the construct separately, followed by an hour incubation for initial adhesion of the cells before adding the culture medium of C2C12.

After five days of culture in the growth medium, the cell constructs were moved to the differentiation medium for another seven days, and the medium was refreshed every other day. Differentiation medium contained ITS (1% v/v). On day 7 of differentiation, unlabeled cells were fixed and double stained with Phalloidin Rhodamine B (100 nM) to stain the actin filaments and anti-sarcomere α -actinin mouse monoclonal 1:200 conjugated with secondary antibody goat anti-mouse IgG-Alexa Fluor 488 1:200 in BSA (0.1%). The nuclei were stained with Hoechst using a 1:1000 dilution. After 1 h of incubation at 37 °C the samples were washed and imaged using confocal microscopy.

Statistical Analysis: All measurements were made at least in triplicates and tested independently. Data were reported as mean values \pm standard deviation. Two-way ANOVA with Bonferroni test was performed for cell culture experiments using Origin 2019b software, and differences were displayed as statistically significant if $p \leq 0.05$. Statistically significant values were presented as * $p \leq 0.05$, ** $p \leq 0.01$, and *** $p \leq 0.001$.

Supporting Information

Supporting Information is available from the Wiley Online Library or from the author.

Acknowledgements

This work was supported by Oberfrankenstiftung (Project-No. 05266). The authors would further like to thank RESORBA for providing collagen grist I/III. S.S. is thankful to DFG (SA 3575/1-1) for financial support. The authors further thank Shakir Bin Zainuddin for fiber spinning support, Annika Lechner for confocal microscopy imaging, David Sonnleitner for SEM imaging of collagen fiber tubes, Prof. Gregor Lang for his advice on mechanical testing, and Dr. Indra Apsite for support in cell culture and SEM. The authors thank Nicholas Chan for proof reading.

Open access funding enabled and organized by Projekt DEAL.

Conflict of Interest

The authors declare no conflict of interest.

Author Contributions

K.S.K. and S.S. contributed equally to this work. K.S.K. and S.S. carried out experimental work and analyzed data; M.H. carried out AFM measurements and helped writing the AFM part of the paper; K.K., S.S., and T.S. wrote the original draft of the manuscript; S.S. acquired funding, conceptualized and supervised the cell study; T.S. acquired funding, conceptualized and supervised the entire study; all authors revised and approved the final version of the manuscript.

Data Availability Statement

The data that support the findings of this study are available from the corresponding author upon reasonable request.

Keywords

braided collagen fibers, continuous fibers, mechanical properties, muscle microtissue, skeletal muscle tissue

Received: November 30, 2021
Published online:

- [1] *Molecular Biology*, (eds.: R. D. B. Fraser, T. P. MacRae), Academic Press, New York **1973**.
- [2] M. Meyer, *Biomed. Eng. Online* **2019**, *18*, 24.
- [3] S. Ricard-Blum, *Cold Spring Harbor Perspect. Biol.* **2011**, *3*, a004978.
- [4] K. E. Kadler, D. F. Holmes, J. A. Trotter, J. A. Chapman, *Biochem. J.* **1996**, *316*, 1.
- [5] M. Kim, W. Kim, G. Kim, *ACS Appl. Mater. Interfaces* **2017**, *9*, 43459.
- [6] R. J. Jakobsen, L. L. Brown, T. B. Hutson, D. J. Fink, A. Veis, *Science (New York, N.Y.)* **1983**, *220*, 1288.
- [7] a) G. Montalbano, S. Toumpaniari, A. Popov, P. Duan, J. Chen, K. Dalgarno, W. E. Scott, A. M. Ferreira, *Mater. Sci. Eng., C* **2018**, *91*, 236; b) N. Pallua, C. V. Suscheck, *Tissue Engineering*, Springer Berlin Heidelberg, Berlin, Heidelberg **2011**.
- [8] S. Zhu, X. Yu, J. You, T. Yin, Y. Lin, W. Chen, L. Dao, H. Du, R. Liu, S. Xiong, Y. Hu, *Food Hydrocolloids* **2021**, *114*, 106576.
- [9] B. Zhu, W. Li, N. Chi, R. V. Lewis, J. Osamor, R. Wang, *ACS Omega* **2017**, *2*, 2439.
- [10] G. Montalbano, C. Tomasina, S. Fiorilli, S. Camarero-Espinosa, C. Vitale-Brovarone, L. Moroni, *Materials* **2021**, *14*, 4360.
- [11] R. Tonndorf, D. Aibibu, C. Cherif, *Mater. Sci. Eng., C* **2020**, *106*, 110105.
- [12] M. T. Arafat, G. Tronci, J. Yin, D. J. Wood, S. J. Russell, *Polymer* **2015**, *77*, 102.
- [13] M. L. Siriwardane, K. DeRosa, G. Collins, B. J. Pfister, *Biofabrication* **2014**, *6*, 015012.
- [14] M. Ebrahimi, S. Ostrovidov, S. Salehi, S. B. Kim, H. Bae, A. Khademhosseini, *J. Tissue Eng. Regener. Med.* **2018**, *12*, 2151.
- [15] D. Puppi, F. Chiellini, *Polym. Int.* **2017**, *66*, 1690.
- [16] a) L. C. Mozdzen, R. Rodgers, J. M. Banks, R. C. Bailey, B. A. C. Harley, *Acta Biomater.* **2016**, *33*, 25; b) C. Rinoldi, E. Kijeńska-Gawrorńska, A. Khademhosseini, A. Tamayol, W. Swieszkowski, *Adv. Healthcare Mater.* **2021**, *10*, 2001305.
- [17] C. Haynl, E. Hofmann, K. Pawar, S. Förster, T. Scheibel, *Nano Lett.* **2016**, *16*, 5917.
- [18] Y. Huang, Y. Wang, L. Chen, L. Zhang, *J. Mater. Chem. B* **2018**, *6*, 918.
- [19] J. M. Caves, V. A. Kumar, J. Wen, W. Cui, A. Martinez, R. Apkarian, J. E. Coats, K. Berland, E. L. Chaikof, *J. Biomed. Mater. Res., Part B* **2010**, *93*, 24.
- [20] M. Meyer, H. Baltzer, K. Schwikal, *Mater. Sci. Eng., C* **2010**, *30*, 1266.
- [21] D. I. Zeugolis, R. G. Paul, G. Attenburrow, *J. Biomater. Sci. Polym. Ed.* **2009**, *20*, 219.
- [22] A. Yaari, Y. Schilt, C. Tamburu, U. Raviv, O. Shoseyov, *ACS Biomater. Sci. Eng.* **2016**, *2*, 349.
- [23] A. Dasgupta, N. Sori, S. Petrova, Y. Maghdouri-White, N. Thayer, N. Kemper, S. Polk, D. Leathers, K. Coughenour, J. Dascoli, R. Palikonda, C. Donahue, A. A. Bulysheva, M. P. Francis, *Acta Biomater.* **2021**, *128*, 186.
- [24] G. Tronci, R. S. Kanuparti, M. T. Arafat, J. Yin, D. J. Wood, S. J. Russell, *Int. J. Biol. Macromol.* **2015**, *81*, 112.
- [25] K. Tomihata, K. Burczak, K. Shiraki, Y. Ikada, in *Polymers of Biological and Biomedical Significance*, American Chemical Society, Washington, DC **1993**, pp. 275–286.
- [26] L. M. Delgado, Y. Bayon, A. Pandit, D. I. Zeugolis, *Tissue Eng., Part B* **2015**, *21*, 298.
- [27] S. Salehi, M. Kharaziha, N. Masoumi, A. Fallahi, A. Tamayol in *Textile Finishing*, (eds.: K. L. Mittal, T. Bahners), John Wiley & Sons, Inc, Hoboken, NJ **2017**, pp. 363–421.
- [28] G. D. Learn, P. E. McClellan, D. M. Knapik, J. L. Cumsky, V. Webster-Wood, J. M. Anderson, R. J. Gillespie, O. Akkus, *J. Biomed. Mater. Res., Part B* **2019**, *107*, 1864.
- [29] A. R. Gillies, R. L. Lieber, *Muscle Nerve* **2011**, *44*, 318.
- [30] S. Jana, S. K. L. Levengood, M. Zhang, *Adv. Mater.* **2016**, *28*, 10588.
- [31] Y. Takagaki, H. Yamagishi, R. Matsuoka, *Int. Rev. Cell Mol. Biol.* **2012**, *296*, 187.

- [32] S. Ostrovidov, X. Shi, R. B. Sadeghian, S. Salehi, T. Fujie, H. Bae, M. Ramalingam, A. Khademhosseini, *Stem Cell Rev. Rep.* **2015**, *11*, 866.
- [33] J. A. Trotter, S. Eberhard, A. Samora, *Cell Motil.* **1983**, *3*, 431.
- [34] T. K. Merceron, M. Burt, Y.-J. Seol, H.-W. Kang, S. J. Lee, J. J. Yoo, A. Atala, *Biofabrication* **2015**, *7*, 035003.
- [35] E. Bianchi, M. Ruggeri, S. Rossi, B. Vigani, D. Miele, M. C. Bonferoni, G. Sandri, F. Ferrari, *Pharmaceutics* **2021**, *13*, 89.
- [36] V. J. Mase, J. R. Hsu, S. E. Wolf, J. C. Wenke, D. G. Baer, J. Owens, S. F. Badylak, T. J. Walters, *Orthopedics* **2010**, *33*, 511.
- [37] a) J. Bruns, *Tissue Engineering*, Steinkopff, Heidelberg **2003**;
b) P. Sharma, N. Maffulli, *J. Bone Joint Surg.* **2005**, *87*, 187;
c) Y. J. No, M. Castilho, Y. Ramaswamy, H. Zreiqat, *Adv. Mater.* **2020**, *32*, 1904511.
- [38] a) M. C. P. Vila Pouca, M. P. L. Parente, R. M. N. Jorge, J. A. Ashton-Miller, *Orthop. J. Sports Med.* **2021**, *9*, 23259671211020731; b) M. Kääriäinen, T. Järvinen, M. Järvinen, J. Rantanen, H. Kalimo, *Scand. J. Med. Sci. Sports* **2000**, *10*, 332.
- [39] H. R. C. Screen, D. L. Bader, D. A. Lee, J. C. Shelton, *Strain* **2004**, *40*, 157.
- [40] N. Narayanan, S. Calve, *Connect. Tissue Res.* **2021**, *62*, 53.
- [41] E. Bayrak, P. Y. Huri, *Front. Mater.* **2018**, *5*, 24.
- [42] W. Yaseen, O. Kraft-Sheleg, S. Zaffryar-Eilot, S. Melamed, C. Sun, D. P. Millay, P. Hasson, *Nat. Commun.* **2021**, *12*, 3852.
- [43] A. Shima, A. Itou, S. Takeuchi, *Sci. Rep.* **2020**, *10*, 288.
- [44] S. T. Cooper, A. L. Maxwell, E. Kizana, M. Ghodussi, E. C. Hardeman, I. E. Alexander, D. G. Allen, K. N. North, *Cell Motil. Cytoskeleton* **2004**, *58*, 200.
- [45] T. G. Mezger, *The Rheology Handbook*, 4th Ed., Vincentz Network, Hannover **2014**.
- [46] H. Mirbaha, P. Nourpanah, P. Scardi, M. D'incau, G. Greco, L. Valentini, S. Bittolo Bon, S. Arbab, N. Pugno, *Materials* **2019**, *12*, 2797.
- [47] K. M. O. Håkansson, A. B. Fall, F. Lundell, S. Yu, C. Krywka, S. V. Roth, G. Santoro, M. Kvick, L. PrahL Wittberg, L. Wågberg, L. D. Söderberg, *Nat. Commun.* **2014**, *5*, 4018.
- [48] M. Humenik, G. Lang, T. Scheibel, *Wiley Interdiscip. Rev. Nanomed. Nanobiotechnol.* **2018**, *10*, e1509.
- [49] S. Salehi, K. Koeck, T. Scheibel, *Molecules (Basel, Switzerland)* **2020**, *25*, 737.
- [50] a) S. Ostrovidov, M. Ebrahimi, H. Bae, H. K. Nguyen, S. Salehi, S. B. Kim, A. Kumatani, T. Matsue, X. Shi, K. Nakajima, S. Hidema, M. Osanai, A. Khademhosseini, *ACS Biomater. Sci. Eng.* **2017**, *3*, 579; b) B. Mirani, E. Pagan, S. Shojaei, S. M. H. Dabiri, H. Savoiji, M. Mehrali, M. Sam, J. Alsaif, R. B. Bhiladvala, A. Dolatshahi-Pirouz, M. Radisic, M. Akbari, *ACS Appl. Mater. Interfaces* **2020**, *12*, 9080; c) A. Fallahi, I. K. Yazdi, L. Serex, E. Leshia, N. Faramarzi, F. Tarlan, H. Avci, R. Costa-Almeida, F. Sharifi, C. Rinoldi, M. E. Gomes, S. R. Shin, A. Khademhosseini, M. Akbari, A. Tamayo, *ACS Biomater. Sci. Eng.* **2020**, *6*, 1112.
- [51] a) S. Ostrovidov, M. Ebrahimi, H. Bae, H. K. Nguyen, S. Salehi, S. B. Kim, A. Kumatani, T. Matsue, X. Shi, K. Nakajima, et al., *ACS Appl. Mater. Interfaces* **2017**, *9*, 42444; b) C. Mueller, M. Trujillo-Miranda, M. Maier, D. E. Heath, A. J. O'Connor, S. Salehi, *Adv. Mater. Interfaces* **2021**, *8*, 2001167.
- [52] S. Ostrovidov, V. Hosseini, S. Ahadian, T. Fujie, S. P. Parthiban, M. Ramalingam, H. Bae, H. Kaji, A. Khademhosseini, *Tissue Eng., Part B* **2014**, *20*, 403.
- [53] C. S. Russell, A. Mostafavi, J. P. Quint, A. C. Panayi, K. Baldino, T. J. Williams, J. G. Daubendiek, V. H. Sánchez, Z. Bonick, M. Trujillo-Miranda, S. R. Shin, O. Pourquie, S. Salehi, I. Sinha, A. Tamayol, *ACS Appl. Bio Mater.* **2020**, *3*, 1568.
- [54] J. W. Sanger, J. Wang, Y. Fan, J. White, J. M. Sanger, *J. Biomed. Biotechnol.* **2010**, *2010*, 858606.
- [55] Y. Xie, J. Chen, H. Celik, O. Akkus, M. W. King, *Biomed. Mater.* **2021**, *16*, 025001.
- [56] a) M. Younesi, A. Islam, V. Kishore, J. M. Anderson, O. Akkus, *Adv. Funct. Mater.* **2014**, *24*, 5762; b) M. Akbari, A. Tamayol, S. Bagherifard, L. Serex, P. Mostafalu, N. Faramarzi, M. H. Mohammadi, A. Khademhosseini, *Adv. Healthcare Mater.* **2016**, *5*, 751.
- [57] a) A. J. Engler, M. A. Griffin, S. Sen, C. G. Bönnemann, H. L. Sweeney, D. E. Discher, *J. Cell Biol.* **2004**, *166*, 877; b) N. M. McKenna, C. S. Johnson, Y. L. Wang, *J. Cell Biol.* **1986**, *103*, 2163.
- [58] a) R. Banan Sadeghian, M. Ebrahimi, S. Salehi, *J. Tissue Eng. Regener. Med.* **2018**, *12*, 912; b) I. Apsite, J. M. Uribe, A. F. Posada, S. Rosenfeldt, S. Salehi, L. Ionov, *Biofabrication* **2019**, *12*, 015016.
- [59] D. G. Hepworth, J. P. Smith, *Composites, Part A* **2002**, *33*, 797.
- [60] J. Gosline, M. Lillie, E. Carrington, P. Guerette, C. Ortlepp, K. Savage, *Philosophical Trans. R. Soc. London, B* **2002**, *357*, 121.
- [61] C. D. Kuthe, R. V. Uddanwadiker, *J. Appl. Biomater. Funct. Mater.* **2016**, *14*, e154.